Journal of Applied Polymer Science

Using Raman spectroscopic imaging for non-destructive analysis of filler distribution in chalk filled polypropylene

Evelin Boros, Peter Bak Porse, Inga Nielsen, Sergey Kucheryavskiy
Section of Chemical Engineering, Department of Chemistry and Bioscience, Aalborg University, Niels Bohrs Vej 8, Esbjerg 6700, Denmark
Correspondence to: S. Kucheryavskiy (E-mail: svk@bio.aau.dk)

ABSTRACT: A feasibility study on using Raman spectral imaging for visualization and analysis of filler distribution in chalk filled polypropylene samples has been carried out. The spectral images were acquired using a Raman spectrometer with 785 nm light source. Eight injection-molded samples with concentration of chalk 25% and 50% were used in the experiment. Two methods for spectral unmixing were applied to the images and both revealed almost identical distribution maps over the samples' surface. The maps also correlated with the ones obtained for several separated peaks, typical for the chalk and the polypropylene. The revealed distribution patterns show the same trend for each concentration level and agree with theoretical explanation of plastic flow into an injection molding tool. © 2015 Wiley Periodicals, Inc. J. Appl. Polym. Sci. **2016**, *133*, 43016.

KEYWORDS: molding; polyolefins; properties and characterization; spectroscopy

Received 23 June 2015; accepted 8 October 2015
DOI: 10.1002/app.43016

INTRODUCTION

Polymer materials have become very important in everyday-life due to their advantageous features compared to conventional materials. Low weight, insulation characteristics, toughness, durability, flame-retardation, and resistance to corrosion can be mentioned among the advantageous properties of polymeric materials.[1]

More than 33% of polymers in plastic industry are produced by injection molding, owing to the feasibility of making complex shapes with high precision, great reproducibility within short periods of time, and cost-effectiveness.[2] Because of the rapid changes in various processing parameters, the material is subjected to different effects. The most significant impacts acting on the material are due to the high-pressure variations and the rapid cooling.[2] These effects, which determine the final products' quality, include[3] polymer properties, product design and characteristics, mold design and configuration, process conditions, as well as injection molding machine and its process control.

Polymer properties include not only the quality of the applied polymeric material, but also the incorporated additives and/or fillers. Use of fillers may have different reasons, but in most of the cases, the main aim is to change physical properties of the raw material. Fillers can also be used for dilution or extension of a polymeric matrix.[4]

The shear forces acting on the material during manufacturing influence the dispersion and distribution of filler particles. In heterogeneously distributed systems, the properties are not even. Local stress maximums evolve around heterogeneous initiating local deformation processes, which might induce premature failure or deteriorated mechanical properties of the product. Furthermore, insufficient distribution can result in poor aesthetics. Therefore, the characterization of filler distribution can be a step towards quality assessment and process optimization.

There are many ways that can be employed to assess the spatial distribution of fillers. However, if a rapid and non-destructive method is needed, the use of vibrational spectroscopy can be particularly beneficial. Vibrational spectroscopic methods, especially near infrared (NIR) and Raman, are used widely for estimation and monitoring of product quality in many areas, first of all in food industry and pharmacy.

There are papers reported on use of the spectroscopic methods on assessing properties of polymer materials and detection of various fillers in polymers, e.g., identification and quantification of calcium carbonate ($CaCO_3$) in compression molded high density polyethylene (HDPE) samples by fourier transformed (FT)-Raman spectroscopy,[5] or characterization of graphene-dispersion in epoxy resins.[6] Most of the studies focused on the dispersion of particles in order to detect higher order structures, which might act as weak sites in the product. Sul *et al.*[7] used

statistical methods to calculate a dispersity index, which gave information about the dispersion and distribution of carbon nanotubes in epoxy resin, based on pictures obtained by Scanning Electron Microscopy (SEM).

Hyperspectral imaging (HIS) is a development of spectroscopic methods allowing to get information about spatial distribution of chemical components. Coupled with methods for multivariate data analysis (chemometrics) it can be very powerful for revealing hidden structures and patterns.[8] The utilization of Raman hyperspectral imaging is one of the most emerging techniques, for example in the pharmaceutical field.

Use of chemometric methods, such as principal component analysis (PCA) and multivariate curve resolution (MCR), is quite efficient for detection of components and the characterization of their distribution by hyperspectral images.[8–10] The combination of such methods is less ubiquitous for polymeric materials, however, the exploitation of the offered advantages has also gained attention in this field. Thus, it was feasible to identify chemically similar polymers, such as polyethylene (PE) and polypropylene (PP),[11] and separate them from other, commonly existing plastic materials in post-consumer waste, such as polyethylene-terephthalate (PET) and poly-vinyl chloride (PVC) by NIR spectral imaging and principal component analysis (PCA).[12] To our knowledge, there are no reports on using spectral imaging for characterization of chalk distribution in PP.

In the present work, Raman spectral imaging has been applied for obtaining distribution patterns of $CaCO_3$ in injection molded PP samples. Visual inspection of spectral images at certain peaks allowed to obtain some interesting patterns. Applying two methods for spectral unmixing made it possible to resolve spectra of PP and the filler and get reliable distribution maps. The article describes a general methodology used to work with spectral imaging for revealing filler distributions as well as main results obtained by using this methodology in our study.

RAMAN SPECTROSCOPY AND SPECTRAL IMAGING

Vibrational spectroscopy is a rapid, non-destructive, and reliable tool for characterization of molecular structure. Infrared (IR) and Raman spectroscopy are the most commonly applied tools for the investigation of the vibrational spectra. Raman spectroscopy uses inelastic scattering of light, which is also referred to as the Raman effect, for getting chemical information for a sample. The incident monochromatic radiation in Raman spectroscopy is in the visible or NIR region, possessing high energy, resulting in greater penetration in comparison with e.g. IR spectroscopy. At the same time, the collected signal is in the mid-infrared spectroscopy (MIR) region, stemming from fundamental vibrations, therefore providing the fingerprint of the molecules.

The collection of spectra can be executed automatically or manually by using the Raman equipment and proper software. The collected Raman spectra of solid surfaces can be organized to form spectral images or *hypercubes*, allowing further analyses of the sample. Spectral image is a collection of spectra at predetermined X-Y positions, followed by repeated measurements with defined distances until the selected area of the sample is investigated.[13] Figure 1 illustrates the structure of a spectral image, which is formed by the collected spectra in X and Y spatial directions with wavenumbers in the Z direction. By having the whole spectrum of wavenumbers in the Z direction, it is possible to choose one or multiple peaks, and create pseudo-color images that represent the intensity of the chosen peaks in the X-Y plane.

The visual analysis of spectral images highly depends on the amount of prior information available regarding the chemical components.[10] If individual spectra of the components are known, the investigation can be carried out based on the characteristic peaks' intensity-distribution throughout the sample. The whole spectrum can also be introduced by classical least squares (CLS) method. However, application of chemometric methods allows to obtain more thorough and reliable results taking into account whole information from the spectra instead of limiting it by considering only individual peaks.

METHODS FOR PREPROCESSING, EXPLORING, AND ANALYSIS OF SPECTRAL DATA

Preprocessing of Raman Spectra

Certain side effects might deteriorate the quality of the spectra, and they should be eliminated prior to any further analysis. The intensity of the Raman scattering is usually weak, therefore parasite signals might significantly influence the results. The undesirable peaks can originate from charge-coupled device (CCD) background noise, cosmic noise, or fluorescence background.[14] They can be eliminated by applying suitable pre-processing techniques. The removal of cosmic spikes is normally carried out by the measurement software, thus the main focus during preprocessing is on the compensation of the varying background due to, among other factors, fluorescence. In the present case the baseline estimation was carried out by asymmetric least squares (ALS) fitting, which relies on curve fitting by asymmetric weights.[15] The method is shortly described below.

The spectra can be divided into regions, which contain analytically significant peaks, and regions without peaks. Baseline estimation with ALS takes into account these regions with different weights, and corrects the expected baseline accordingly. It is based on the minimizing of the following function:

$$Q = \sum_i v_i (y_i - f_i)^2 + \lambda \left(\Delta^2 f_i\right)^2 \quad (1)$$

where y represents the data (spectrum), f is a smooth trend (i.e. the expected baseline), v is prior weights, and λ is roughness penalty. If $y > f$, i.e. there is a peak above the expected baseline, $v = p$. On the contrary, if the data is below or on the expected baseline, $v = 1 - p$ with $0 < p < 1$, therefore, positive and negative deviations from the trend get different weights. The parameter λ determines the contribution of the second term. The greater λ is, the smoother f gets.[15]

Another important preprocessing step is a normalization of the spectra. Normalization allows to get rid of physical effects (such as e.g. different focal distance due to an uneven surface of a sample) in the spectra without changing relationships among the spectral peaks. There are several ways to normalize the spectra: unit area, unit length, or standard normal variate (SNV) normalization. In the present work, a unit length normalization

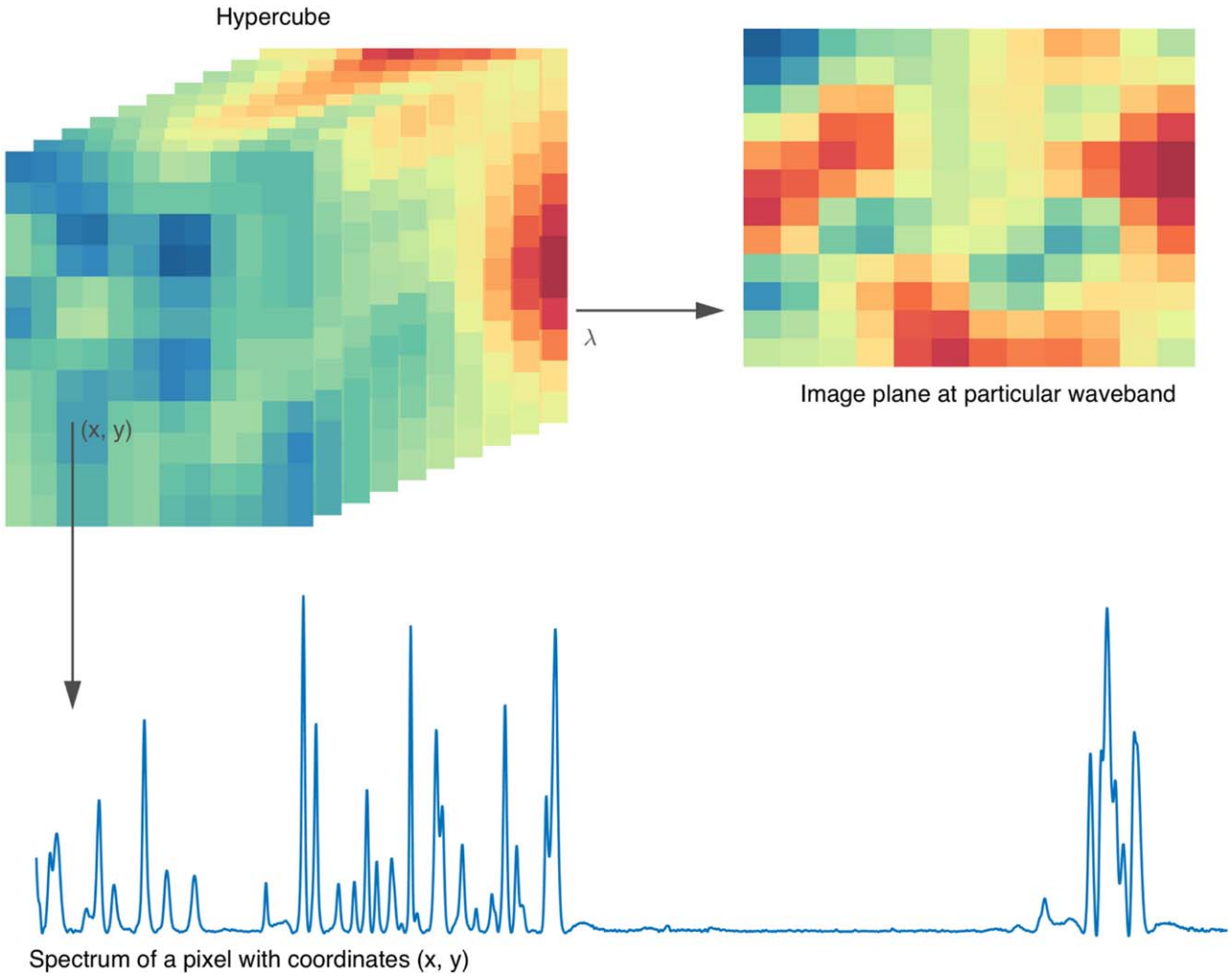

Figure 1. Spectral image (a hypercube). [Color figure can be viewed in the online issue, which is available at wileyonlinelibrary.com.]

was utilized, so every spectrum was represented as a unit vector in spectral (wavenumber) multidimensional space.

Multivariate Curve Resolution

In order to obtain more accurate information about the substances of the sample, i.e. their spectra and relative concentration profiles, spectral unmixing can be applied, which is referred to as Multivariate Curve Resolution (MCR) in chemometrics. This approach is based on the fact that each pixel of the hyperspectral image is a linear combination of several spectral signatures of different materials (namely individual spectra of components). By spectral unmixing, it is possible to decompose the pixels' spectra into a collection of constituent spectra and the corresponding proportion of each material even if the mixture is unknown.[16] Two methods for spectral unmixing have been applied in this work—SIMPLISMA (SIMPLe-to-use Interactive Self-modeling Mixture Analysis) and Multivariate Curve Resolution with Alternating Least Squares (MCR-ALS).

The SIMPLISMA is a simple and fast self-modelling method for spectral unmixing, which does not require reference spectra or any other prior information. The SIMPLSIMA algorithm has been invented by Willem Windig[17] and was improved later by the author and his colleagues.[17] The algorithm is iterative and based on a so-called *purity approach*. It assumes that the analyzed spectra have wavenumbers, which mostly experienced contribution of only one of the chemical components, so the variation of spectral intensity at this wavenumber is directly connected to the concentration of a particular component. These wavenumbers are called *pure variables*. If at least one pure variable is found for each component, then the pure spectra for the components can be found by a linear regression.

The pure variables are identified by a *purity function,* which is a ratio of standard deviation of pixel intensity to the mean intensity calculated separately for each wavenumber. In order to tackle problem with zero mean a small constant value is added to the denominator. The values can be plotted as a function of wavenumbers and is called *purity spectrum*.

The algorithm works as following. First, a purity function is calculated for the original spectral data. The maximum for the purity function points out the pure variable of the strongest component. The pure spectrum of the component is evaluated and its influence is eliminated from the data. Then the steps are repeated to find the next component.

The original algorithm has an important drawback, since for complicated mixtures it is rather difficult to find a waveband, where influence of mixture components is not overlapped. This problem can be tackled by using a modified algorithm, where a second derivative is used instead of original signal, since the derivative may significantly improve resolution of overlapped peaks, keeping the linearity at the same time.

MCR-ALS is another widely used soft-modeling technique for the decomposition of two-way data sets.[18] In the present study, it was applied for spectroscopic data, organized into the data matrix **D**. The decomposition of this matrix is carried out according to eq. 2[19]:

$$D = CS^T + E \quad (2)$$

where C represents the concentration of the species involved, S describes the spectra of pure components, while E stands for the residual matrix. The decomposition of the data matrix into matrices containing the spectra and the corresponding concentrations is feasible due to the assumption that the collected signals follow a bilinear additive model (Lambert-Beer Law).[19]

Many sets of **C** and $\mathbf{S^T}$ are able to describe the original data matrix; therefore, different constraints have to be applied during the ALS optimization to avoid ambiguities. One of the most commonly used constraints is non-negativity[19]—either spectra or concentrations or both may not have negative values. The implementation of other constraints can considerably help the analysis, such as the introduction of chemical information as an equality constraint if the pure components' spectra are available.[20] Further possibilities for constraints include unimodality, closure, trilinearity, selectivity, and/or other shape- and hard-modeling constraints.[21]

Equation (2) is solved iteratively by an ALS method for proposed number of components, by using initial estimation of either **C** or $\mathbf{S^T}$.[21] Convergence is achieved, if the difference in standard deviations between the calculated and experimental data values is less than a certain value in two following iteration steps.[21]

All calculations, modelling, and plotting in the present work have been carried out using MATLAB® R2015a (The MathWorks, Natick, Massachusetts), for MCR-ALS a toolbox written by chemometric group from University of Barcelona was used.[21]

EXPERIMENT AND RESULTS

Materials

Chalk-filled PP samples with different filler concentrations (25% and 50% chalk by mass concentration) were investigated during the experiments. Two samples of each concentration were chosen for analysis with manual mapping.

The 50% chalk content was provided by a supplier, while 25% chalk content was obtained by diluting this material with pure PP by means of a twin-screw extruder (LabTech Engineering), cooled with water, and grinded by a pelletizer machine into 3 mm pellets. The production of samples was performed by injection molding (ENGEL victory 60). The mold produced a thin sample of rectangular shape. The samples' size was approximately 35 mm × 30 mm with thickness of about 1 mm.

Experiment

The experiments were carried out using analyzing unit RamanRXN1 with 785 nm laser source from Kaiser Optical Systems. The wavenumber range of the collected spectra was from 100 to 3500 cm^{-1} with spectral resolution of 1 cm^{-1}. The laser power was set to 400 mW.

The generated laser beam from the laser source was directed through a fiber optical cable to the non-contact probe, where it illuminated the sample at approx. 1 cm distance from the probe. The backscattered radiation was collected by the same probe and directed through the cable to the notch filter that removed Rayleigh scattering. The radiation went afterwards to the monochromator, which separated the light before it reached the CCD detector.

The collection of spectra from the surface of a sample was performed manually by moving the sample by 0.5 cm in X and Y directions, which resulted in a spectral image with 7 × 6 pixels (42 spectra). The spectra acquisition was carried out with exposure time = 3 s, the laser spot size was around 0.3 cm with 0.5 cm between the centers of the spots.

The obtained spectra showed the intensity as a function of wavenumber. Prior to further analysis the spectra were cut to 140...3200 cm^{-1} to remove noisy tails and pre-processed with ALS baseline correction. The parameters of the baseline correction algorithm were found experimentally as the following: smoothness: 1000 and penalty: 0.002. After that, spectra were normalized to a unit length by dividing the spectral values to square root of sum of squared intensities. Figure 2 shows spectra for four samples (two with 25% chalk and two with 50% chalk) before (left) and after (right) the preprocessing.

Exploratory Analysis of Spectral Images

In Figure 3 spectra of the pure components, $CaCO_3$ and PP are shown. One can see that $CaCO_3$ has two clear peaks at 280 cm^{-1} and 1086 cm^{-1} while PP has one of the strongest peak at 809 cm^{-1}. All three peaks are very much selective, meaning that the other component has almost no Raman signal at the wavebands. Investigation of the preprocessed spectra acquired for the samples (Figure 2) showed that the samples with 25% of $CaCO_3$ had chalk peaks, whose size was about two times smaller in comparison with samples having 50% of $CaCO_3$. It can be also noted that the variation of the spectra within each sample is very small, which might be a good illustration of the samples' homogeneity in the investigated layer.

In order to see the spatial distribution of the Raman intensities and, therefore, the concentration of components, a set of pseudo-color images was made for each of the selected peaks as shown in Figure 4. The first two rows show images corresponding to the chalk peaks (280 cm^{-1} and 1086 cm^{-1}), whereas images in the third row correspond to the PP peak at 809 cm^{-1}. Since the average concentration of chalk in the samples was known, we rescaled the peak height to the concentration of the chalk in percent by using simple linear regression, so the color bar legends for these images show the estimated concentration. The images for 809 cm^{-1} use original scale, which corresponds to the peak height. A missing segment on each

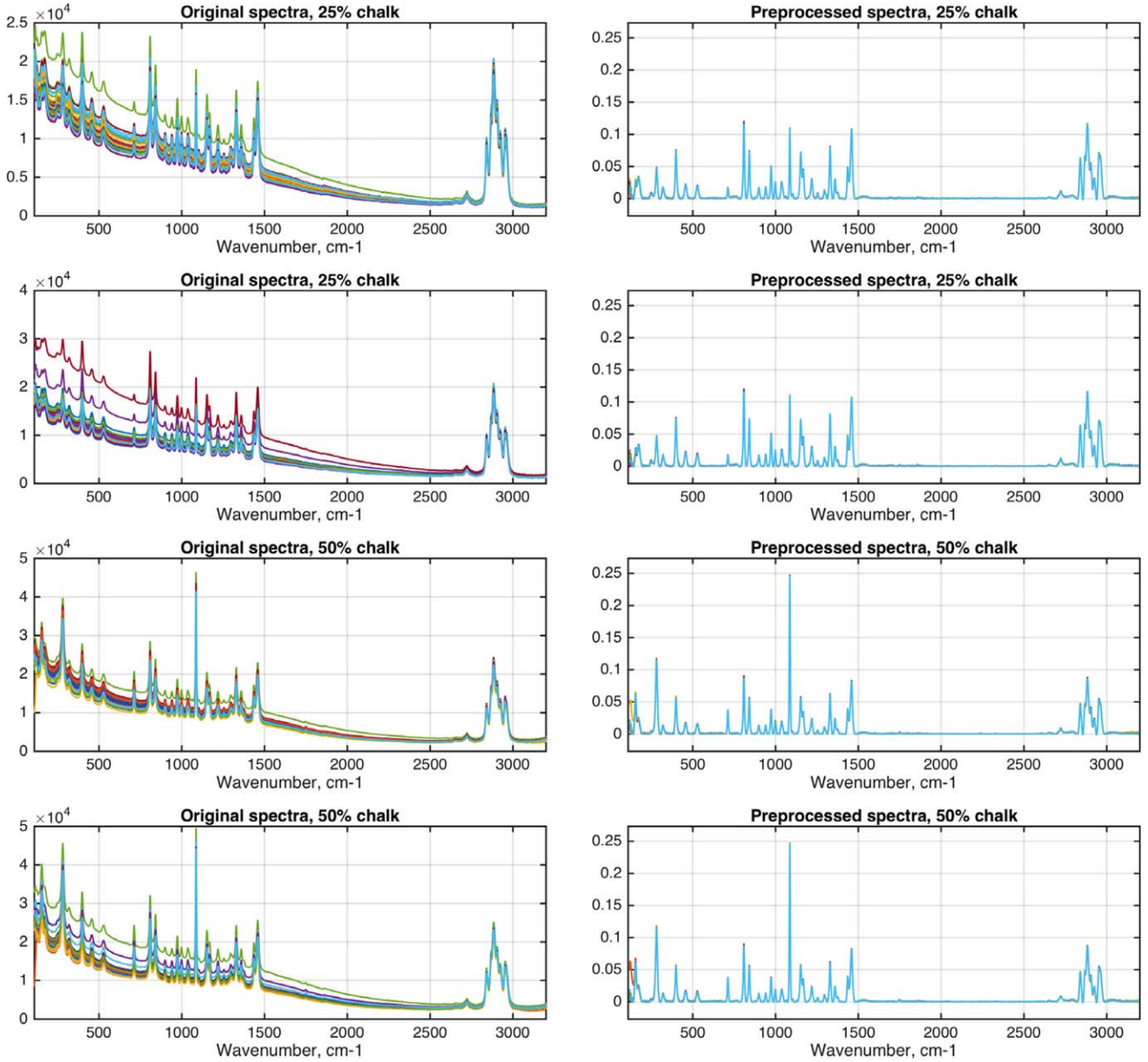

Figure 2. Original (left) and preprocessed (right) spectra from four selected samples. [Color figure can be viewed in the online issue, which is available at wileyonlinelibrary.com.]

image indicates the gate position on the sample, where a hole could be found on the product, therefore the data acquisition performed on that segment was always treated as an outlier.

Generally, it can be seen that the shown patterns are very similar for the samples with the same filler concentration and there is a clear difference between the samples with lower (25%) and higher (50%) concentration. In both cases, spatial variation of the filler is very small (around 1% of the average concentration). Also, as expected, concentrations of filler and PP are complementary.

In order to see the spatial distribution of the filler in all samples better the images for peaks, corresponding to the chalk, were rescaled according to the average concentration, so for 25% samples, the scale was approximately from 19% to 21% and for the 50% samples, the scale was between 48% and 52%. The intensities for PP peak (809 cm^{-1}) were not rescaled, however, individual limits for the intensity levels for 25% and 50% case were used in this case. The images are shown in Figure 5. The deviation of values shown by the scales and the theoretical values might have been caused by minor errors during the measuring, mixing, and production of samples.

The comparatively small amount of spectra taken for each sample makes the images look "pixelized" and complicates visual analysis. On the other hand, taking more spectra requires more time and more precise (and expensive) equipment for positioning of the samples. It was decided to tackle this problem by using bicubic interpolation as it is shown in Figure 6. Bicubic

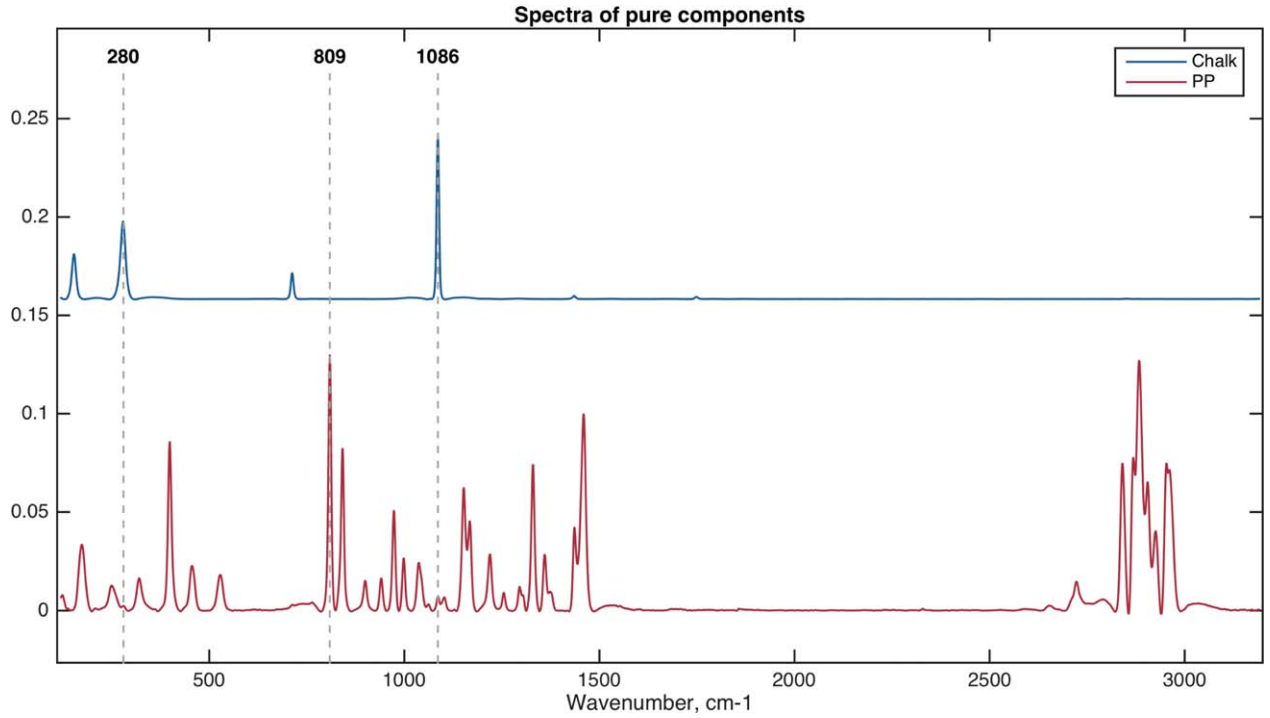

Figure 3. Spectra of pure chalk and polypropylene. [Color figure can be viewed in the online issue, which is available at wileyonlinelibrary.com.]

interpolation[22] is an extension of interpolation of points with cubic polynomial to a two-dimensional case where points are located in a two-dimensional grid. It allows to upsample image pixels in order to tackle the effect of pixelization on low-resolution images. The interpolated images reveal the patterns better and therefore allow to make the visual analysis more comprehensive.

The interpolated images show that samples with the same concentration of the filler clearly share the same trend in their spatial distribution. Also, the variation for 50% samples is smaller,

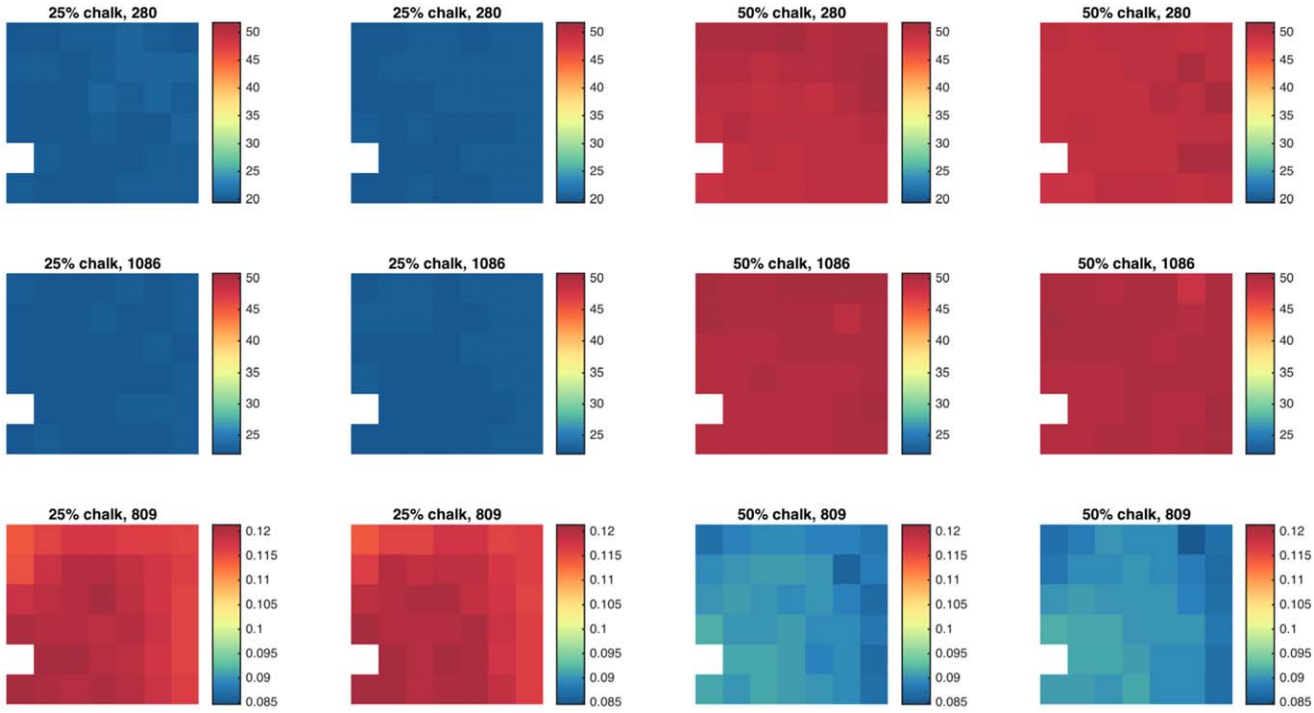

Figure 4. Raman intensity at the selected wavebands shown as pseudo-color images. [Color figure can be viewed in the online issue, which is available at wileyonlinelibrary.com.]

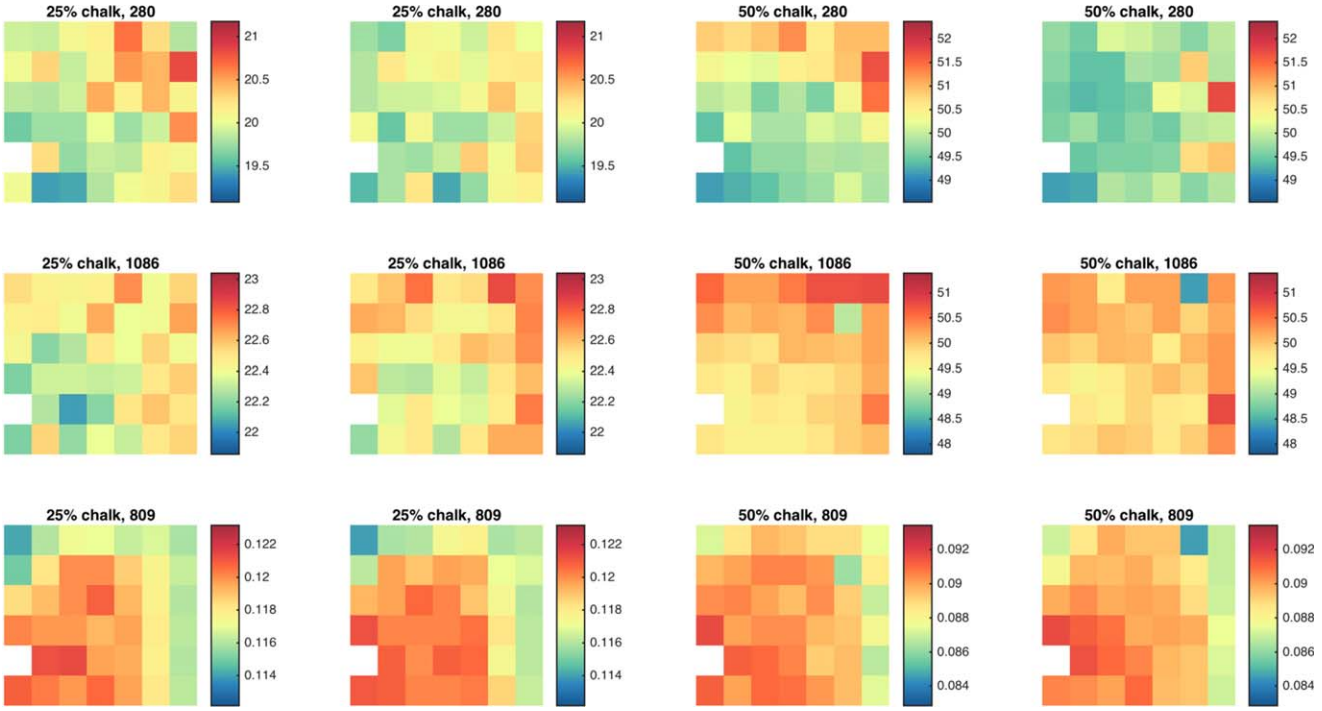

Figure 5. Raman intensity images with individual scales for color gradient. [Color figure can be viewed in the online issue, which is available at wileyonlinelibrary.com.]

as it can be specifically noticed for the 1086 cm^{-1} wavenumber images. This could be due to the fact that this concentration was obtained by the supplier, while the 25% concentration has been reached by compounding the material with a twin-screw extruder, possibly resulting in less sufficient mixing of the filler particles in the polymer matrix.

The appearing blue specks on the right top side of samples can be an indication of mechanical impact on the sample surface.

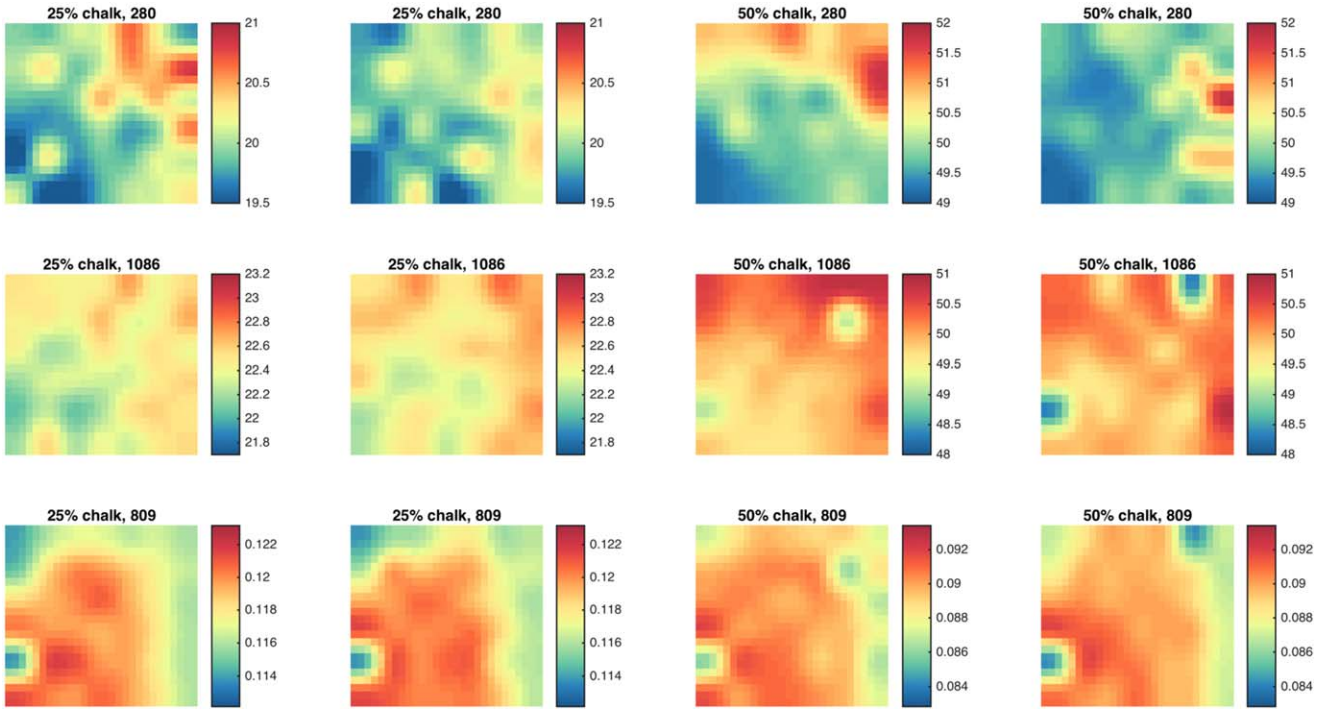

Figure 6. Raman intensity images with individual scales after interpolation. [Color figure can be viewed in the online issue, which is available at wileyonlinelibrary.com.]

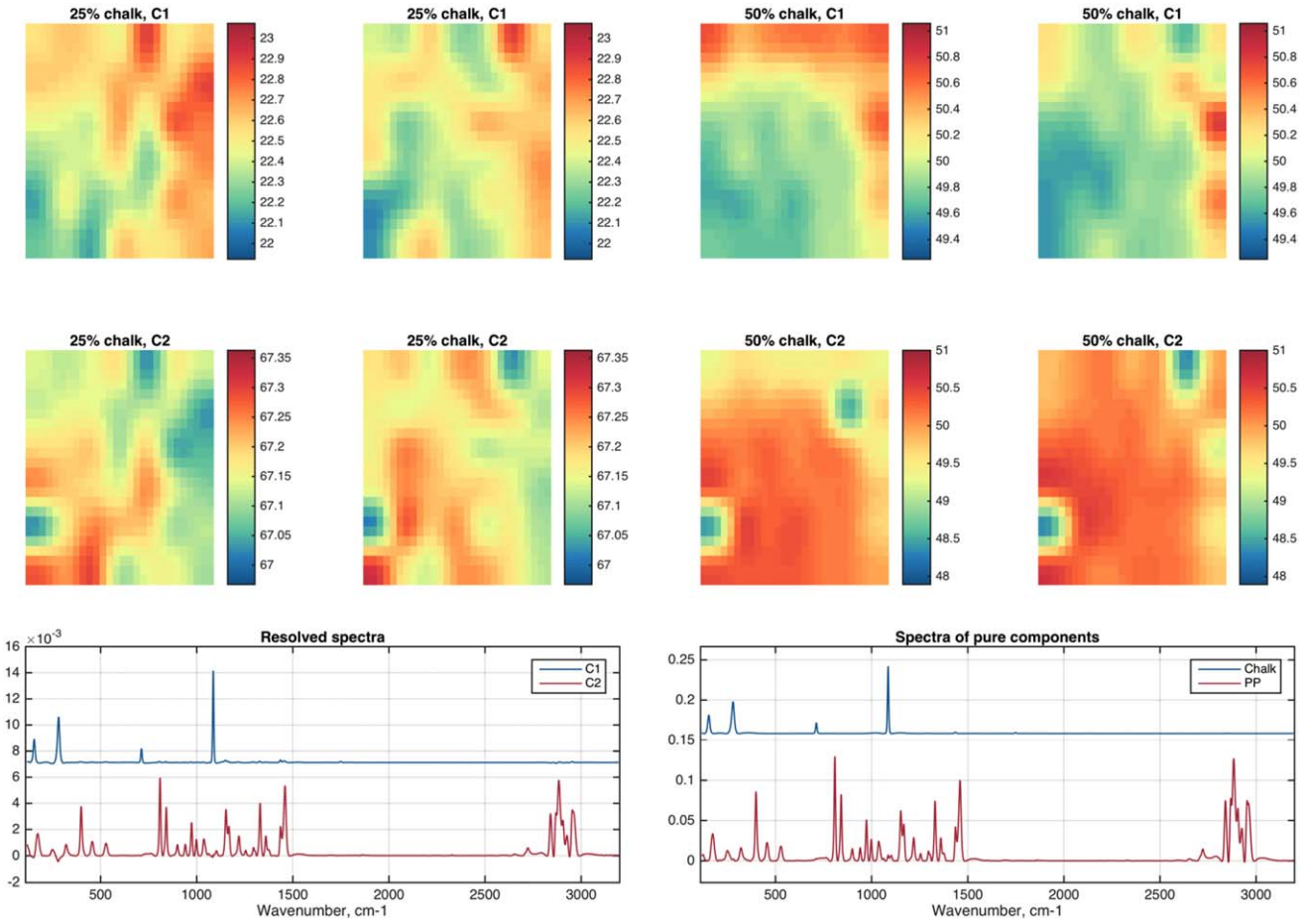

Figure 7. Spectra of resolved components (bottom) and concentration maps (middle and top) obtained with SIMPLISMA. [Color figure can be viewed in the online issue, which is available at wileyonlinelibrary.com.]

As long as it appears approximately at the same position of each image, it can feasibly be linked to a systematic effect. This is the area, where the ejector pins of the injection molding tool had touched the sample during production. The fact that this mechanical impact can be seen on the images points out that Raman spectroscopy has probed the surface area of the samples.

The relative heterogeneity of filler distribution is due to the constantly changing conditions and complicated flow patterns during injection molding of polymers. It is out of the scope to carry out detailed investigation of the evolved flow patterns. Generally, the simulation of flow in an injection molding tool requires complex tools. As it was mentioned in the Introduction, numerous factors have to be taken into account during this processing technique, which influence the flow of the polymer melt and therefore the product quality. Besides that, fillers also have an effect on the material flow, further complicating the calculations.

It can also be seen that for all samples concentration of the filler is a bit larger for the pixels, which are far from the gate position, while the concentration of PP clearly shows the opposite trend. Even though the difference in concentration at the different positions is not very significant, it might be an indication of the specific flow pattern in the injection molding tool.

The general pattern of material flow into a mold shows that a spherical volume of material in the melt front is stretched into an ellipsoid shape as it advances.[23] Thus the molecular chains are stretched. Close to the cold wall, this orientation freezes immediately as the hot polymer melt touches the cold surface. At the same time in the direction towards the middle of the wall thickness—due to the bad thermo-conductivity of polymers—the molecule chains remain mobile for a longer period of time, allowing to relaxation of the stretched molecules. Consequently, the properties change in this dimension (thickness) as well of the product, not only to the flow direction. It is, therefore, important to know the penetration depth of the laser, when investigating such patterns in order to make reliable conclusions about the spatial distribution.

Analysis of Spectral Images by MCR

Exploratory analysis of the spectral images at selected wavebands has shown clear patterns. However, the obtained images with distribution patterns take into account only one peak of the Raman spectra. A more precise overview could be obtained about the differences of the probed areas if more information provided by the spectra was considered. Therefore, multivariate curve resolution of the hypercubes was carried out. Both SIMPLISMA and MCR-ALS methods were applied to the images. In

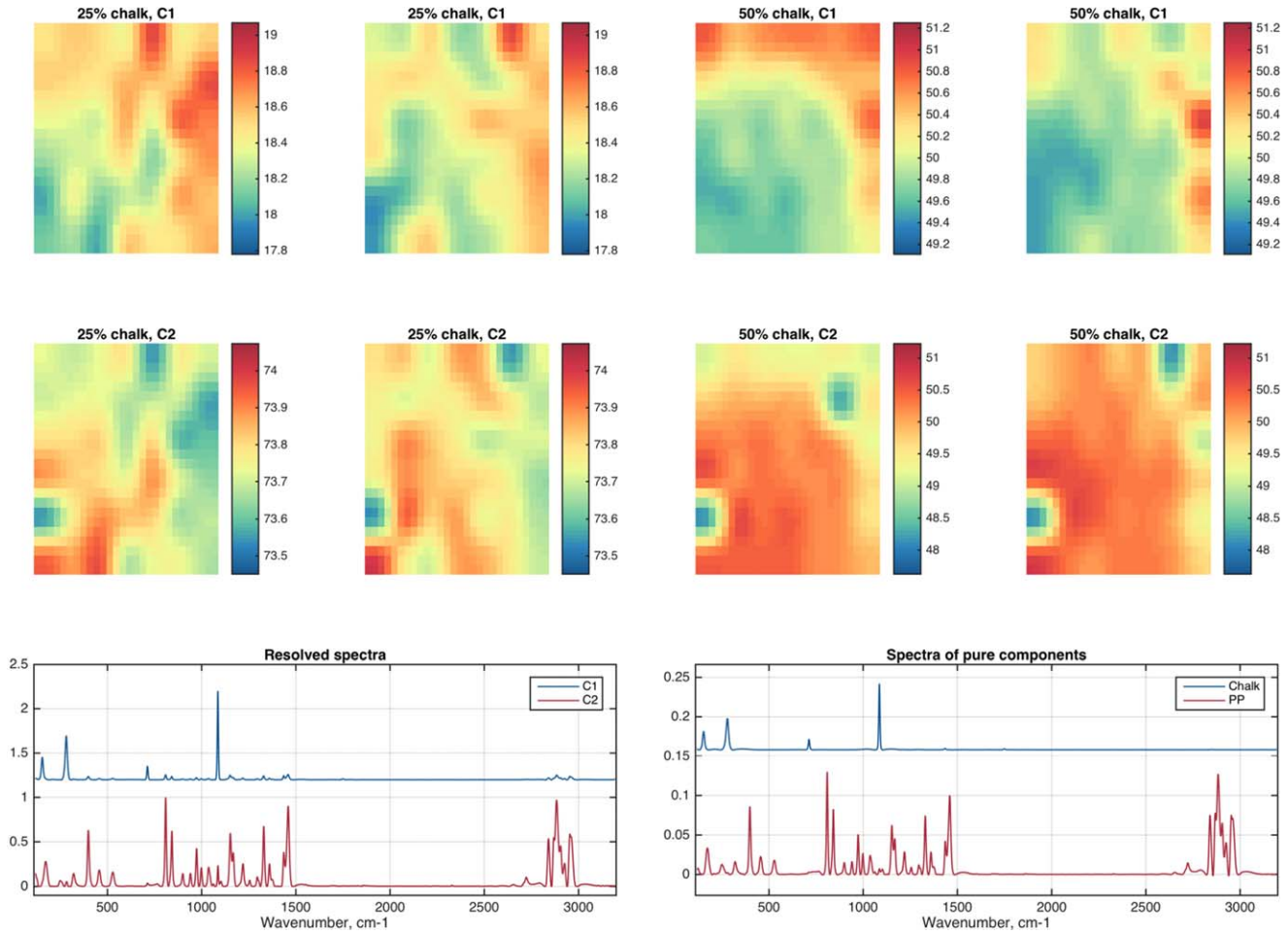

Figure 8. Spectra of resolved components (bottom) and concentration maps (middle and top) obtained with MCR-ALS. [Color figure can be viewed in the online issue, which is available at wileyonlinelibrary.com.]

order to provide more information to the methods the spectral images were merged into a big image before the analysis and the obtained concentration matrix was split up to the individual parts right after. Both methods have been looking for two chemical components (namely C1 and C2).

For the SIMPLISMA algorithm a second derivative was obtained using Savitzky-Golay filter with filter width = 5 and cubic polynomial, and then used instead of original spectra for resolving. The resolved spectra of the pure components as well as the pseudo-color images with concentration maps are shown in Figure 7.

At the bottom of the figure a plot with the resolved spectra (left) and the original spectra of Chalk and PP (right) are presented. It can be clearly seen that spectrum for the first resolved component, C1, corresponds to the spectrum of chalk, whereas the spectrum of the second component, C2, to the spectrum of PP. Despite small disturbances such as a negative peak for C2 around 250 cm^{-1}, the resolved spectra in general resemble the spectra of the pure components almost ideally.

The pseudo-color images in the middle and the top part of the figure represent concentration maps with individual scales for each sample (similar to images shown in Figures 5 and 6 for selected wavebands). In general, the concentration patterns look very close to the ones obtained for individual peaks, which in this case was expected, as the characteristic peaks of the two components do not overlap. However, even in this case, it can be noticed that the patterns obtained with SIMPLISMA are smoother and reveal better the complimentary nature of C1 and C2 distributions.

For MCR-ALS, it was decided to use non-negativity constrains for both concentration and spectral values. PCA was applied prior to curve resolution procedure to get vectors with loadings for first two principal components, which were utilized as initial estimates for the resolved spectra. The MCR-ALS converged after 74 iterations resulted with 99.9% of explained variance. The resolved spectra as well as the concentration maps are shown in Figure 8 (the plots are organized the same way as for SIMPLISMA).

The resolved spectra have no negative peaks in this case due to the used constrains. However, for example spectrum for C1, which also corresponds to the spectrum of chalk, reveals small peaks typical for PP and vice versa. On the other hand, the magnitude of these peaks is very small and should not have a significant influence. The concentration maps reveal almost identical patterns compared to the SIMPLISMA results, however, showing small difference in concentration scale. If one

compares the difference between the pixels with largest and smallest values for the concentration maps, both methods give around 1.0–1.1%.

CONCLUSIONS

The results obtained using two different methods for multivariate curve resolution have shown almost identical distribution patterns as well as have given resolved spectra qualitatively very close to the theoretical spectra of pure components—chalk and PP in this case. From our point of view, this first of all tells about a good stability and reliability of the selected methodology. The use of soft-modelling approach for resolving the spectra allowed to obtain results without having experimental spectra of pure components.

The results can be further improved by adjusting an acquisition equipment. Thus when acquiring the spectral images, it should be taken into account that the area of the actual measurements (laser spot size) is in reality quite small (typically 2–3 mm in diameter or even less), therefore, each pixel represents only a fraction of the corresponding area. These uncertainties could be avoided by the application of a specific probe, which takes several spectra from the adjacent points and returns an average of them.

Another important issue is a penetration depth, which depends on several things, first of all the wavelength of the excitation light, its power and optical system used for focusing. A full control of all four parameters is necessary for reproducibility.

In general, the obtained results allow us to conclude that the use of Raman spectroscopic imaging coupled with proper methods for preprocessing and analysis of the obtained spectra gives an efficient tool for non-destructive, reliable, and rapid estimation of spatial distribution of fillers in injected molded shapes and for assessing their homogeneity in the probed layer. This technique might be particularly useful for example in the assessment and comparison of different mixing techniques even if the spectra of pure components are not available.

REFERENCES

1. Chanda, M.; Roy, S. K. Plastics Technology Handbook, 4th ed.; CRC Press: Boca Raton, Florida, **2006**.
2. Chen, Z.; Turng, L. S. *Adv. Polym. Technol.* **2005**, *24*, 165.
3. Zhou, H., Ed. Computer Modeling for Injection Molding: Simulation, Optimization, and Control, 1st ed.; Wiley: Hoboken, New Yersey, **2013**, p 19.
4. Hornsby, P. R. *Adv. Polym. Sci.* **1999**, *139*, 155.
5. Pakjamsai, C.; Suwanprateeb, J. *J. Appl. Polym. Sci.* **2000**, *78*, 1947.
6. Shojaee, S. A.; Zandiatashbar, A.; Koratkar, N.; Lucca, D. *Carbon N. Y.* **2013**, *62*, 510.
7. Sul, I. H.; Youn, J. R.; Song, Y. S. *Carbon N. Y.* **2011**, *49*, 1473.
8. Boiret, de Juan, M.; Gorretta, A. N.; Ginot, Y. M.; Roger, J. M. *J. Pharm. Biomed. Anal.* **2014**, *103*, 35.
9. Vajna, B.; Patyi, G.; Nagy, Z.; Bódis, A.; Farkas, A.; Marosi, G. *J. Raman Spectrosc.* **2011**, *42*, 1977.
10. Vajna, B.; Farkas, A.; Pataki, H.; Zsigmond, Z.; Igricz, T.; Marosi, G. *Anal. Chim. Acta* **2012**, *712*, 45.
11. Serranti, S.; Gargiulo, A.; Bonifazi, G. *Waste Manag.* **2011**, *31*, 2217.
12. Hu, B.; Serranti, S.; Fraunholcz, N.; Di Maio, F.; Bonifazi, G. *Waste Manag.* **2013**, *33*, 574.
13. Mcgarvey, J. J.; Beattie, J. R. In Raman Imaging; Zoubir, A., Ed.; Springer: Berlin, Heidelberg, **2012**; Vol. *168*.
14. Bocklitz, T.; Walter, A.; Hartmann, K.; Rösch, P.; Popp, J. *Anal. Chim. Acta* **2011**, *704*, 47.
15. Eilers, P. H. C. *Anal. Chem.* **2004**, *76*, 404.
16. Zhang, X.; Tauler, R. *Anal. Chim. Acta* **2013**, *762*, 25.
17. Windig, W.; Guilment, J. *Anal. Chem.* **1991**, *63*, 1425.
18. Mouton, N.; Devos, O.; Sliwa, M.; de Juan, A.; Ruckebusch, C. *Anal. Chim. Acta* **2013**, *788*, 8.
19. Ulrici, A.; Serranti, S.; Ferrari, C.; Cesare, D.; Foca, G.; Bonifazi, G. *Chemom. Intell. Lab. Syst.* **2013**, *122*, 31.
20. Garrido, M.; Rius, F. X.; Larrechi, M. S. *Anal. Bioanal. Chem.* **2008**, *390*, 2059.
21. Jaumot, J.; Gargallo, R.; De Juan, A. A graphical user-friendly interface for MCR-ALS: A new tool for multivariate curve resolution in MATLAB **2005**, *76*, 101.
22. Keys, R. *Acoust. Speech Signal Process.* **1981**, *29*, 1153.
23. Fischer, J. M. Handbook of molded part shrinkage and warpage, William Andrew: Norwich, NY, **2003**.